PHYSICAL REVIEW D VOLUME 23, NUMBER 9 1 MAY 1981

Proton-helium elastic scattering from 45 to 400 GeV*

A. Bujak,[†] P. Devensky,[‡] A. Kuznetsov, B. Morozov, V. Nikitin, P. Nomokonov, Yu. Pilipenko, and V. Smirnov
Joint Institute for Nuclear Research, Dubna, U.S.S.R.

E. Jenkins
University of Arizona, Tucson, Arizona 85721

E. Malamud, M. Miyajima,[§] and R. Yamada
Fermi National Accelerator Laboratory, Batavia, Illinois 60510

(Received 17 June 1980)

The elastic proton-helium differential cross section has been determined for incident laboratory energies from 45 to 400 GeV in the range $0.003 \le |t| \le 0.52$ $(\mathrm{GeV}/c)^2$ by means of the internal-gas-jet-target technique. The differential cross section drops 4–5 orders of magnitude to the first dip at $|t| \simeq 0.22$ $(\mathrm{GeV}/c)^2$. The shrinkage in the slope of the differential cross section is found to be twice as fast as that in the proton-proton case. The slope parameter at $|t| \simeq 0$ is described by the formula $b = 24 + 1.13 \ln s$, where b is in $(\mathrm{GeV}/c)^{-2}$ and s is in GeV^2. The elastic proton-helium cross section is normalized to the known elastic proton-proton cross section using data taken with a helium and hydrogen mixture as a target. The proton-helium total cross section is determined from the optical theorem. The total cross section rises by 4% between 100 and 400 GeV. Results are presented on the real part of the elastic-scattering amplitude and on the total elastic cross section. The experimental differential cross sections are compared to Glauber-model predictions.

I. INTRODUCTION

Previous studies of proton-helium elastic scattering have been made at low and intermediate energies.[1] Results at 24 GeV/c have been reported.[2] An experiment on the inverse reaction ^{4}He-proton elastic scattering at 1.75, 2.51, and 4.13 GeV/nucleon has also been reported.[3,4] The measurements of $e\,^4$He up to 1 GeV/c (Refs. 5 and 6) and of π^-He at 7.76 GeV/c (Ref. 7) are available in the literature. All these experiments exhibit a diffraction minimum or dip in the differential cross section. Such a structure is more pronounced at higher energies.

There are several theoretical models capable of describing the shape of the differential cross section.[8,9] Czyż, Leśniak, and others[10–12] have developed the Glauber multiple-scattering model extensively. In this model the first minimum arises due to the interference between the single ($k=1$) and multiple ($k=2, 3, 4,$) scattering of the incident particle inside the nucleus. The $k=1$ and $k=2$ imaginary amplitudes cancel at the diffraction minimum. What remains is the coherent sum of the real amplitudes for $k=1$–4, imaginary amplitudes ($k=3, 4$), spin effects and, for $k=2, 3, 4$ scattering, the amplitudes for the processes going through intermediate inelastic states. The ^{4}He is the most compact light nucleus. In the case of $p\,^4$He collisions, inelastic rescattering is expected to be much larger than in another light nucleus. Thus, comparison of the results of proton-proton, proton-deuteron, and proton-helium scattering experiments is a promising way to estimate the most important corrections to the Glauber multiple-scattering model.

In Sec. II we describe the experiment and details of the analysis. The method of absolute normalization of the differential cross section is presented in Sec. III. In Sec. IV and Table I we present our proton-helium data at 45, 97, 146, 200, 259, 301, and 393 GeV. The 45-GeV data was originally taken as two separate experiments at 44.9 GeV and 45.5 GeV. In the differential cross sections shown in Table I, these two sets of data have been averaged. The figures and tables derived from fits to the differential cross sections preserve these data as two independent points and illustrate the reproducibility of the data.

The results of the fits to the low-$|t|$ region are discussed in Sec. V. The tables with a list of parameters include the slope $b(s)$, the t-dependence of the slope, the real part of the amplitude at $|t|=0$, the total $p\,^4$He cross section, and the s dependence of all the above parameters using a linear approximation. In Sec. VI we compare the Glauber-model predictions to the data in the entire t region including the diffraction dip. In Sec. VII we summarize the results.

II. EXPERIMENTAL APPARATUS AND DATA ANALYSIS

The experimental apparatus is shown in Fig. 1. The Fermilab circulating proton beam intercepts a gas target with an average thickness of 4×10^{-7}

TABLE I. $d\sigma/dt$ differential cross sections for elastic $p\,{}^4$He scattering at 45, 97, 146, 200, 259, 301, and 393 GeV. Errors are only statistical, and the error in absolute normalization is ±4.8% as stated in the text.

$-t$ [(GeV/c)^2]	$d\sigma/dt$ [mb/(GeV/c)^2]	$-t$ [(GeV/c)^2]	$d\sigma/dt$ [mb/(GeV/c)^2]
45 GeV			
0.003 38	760.4 ± 8.5	0.101 16	24.4 ± 0.2
0.004 73	700.5 ± 7.0	0.103 87	21.2 ± 0.4
0.005 81	670.2 ± 12.5	0.106 71	19.9 ± 0.3
0.006 32	657.4 ± 5.3	0.111 83	16.6 ± 0.2
0.007 62	593.4 ± 10.3	0.121 21	11.6 ± 0.2
0.008 15	597.3 ± 3.9	0.126 63	9.19 ± 0.12
0.010 31	555.7 ± 5.4	0.136 06	6.52 ± 0.14
0.010 72	547.3 ± 9.2	0.142 15	4.95 ± 0.09
0.011 16	535.9 ± 4.9	0.147 43	3.62 ± 0.05
0.011 68	540.6 ± 5.4	0.152 08	3.22 ± 0.10
0.012 50	515.2 ± 6.3	0.158 57	2.19 ± 0.05
0.013 02	510.4 ± 6.9	0.163 94	1.73 ± 0.03
0.013 26	500.7 ± 7.9	0.175 81	0.993 ± 0.030
0.014 07	491.2 ± 4.6	0.181 13	0.686 ± 0.014
0.014 74	478.2 ± 4.0	0.189 30	0.458 ± 0.016
0.015 10	454.7 ± 5.8	0.192 43	0.334 ± 0.016
0.015 53	464.7 ± 6.6	0.193 23	0.334 ± 0.016
0.015 80	458.5 ± 6.2	0.198 24	0.256 ± 0.015
0.016 04	471.6 ± 7.8	0.198 97	0.197 ± 0.020
0.018 15	423.4 ± 3.3	0.199 10	0.189 ± 0.019
0.018 92	411.7 ± 2.1	0.200 36	0.234 ± 0.018
0.021 22	376.3 ± 4.7	0.200 94	0.162 ± 0.019
0.021 90	372.1 ± 3.7	0.201 73	0.171 ± 0.017
0.022 65	366.6 ± 5.1	0.201 81	0.180 ± 0.011
0.023 78	350.9 ± 3.0	0.202 57	0.150 ± 0.013
0.025 02	336.5 ± 3.7	0.212 60	0.0760 ± 0.0084
0.026 07	329.9 ± 4.8	0.213 45	0.0644 ± 0.0108
0.026 43	318.1 ± 4.1	0.213 49	0.0549 ± 0.0071
0.027 57	312.3 ± 3.0	0.214 89	0.0586 ± 0.0066
0.028 75	296.8 ± 1.9	0.216 30	0.0571 ± 0.0063
0.031 83	268.0 ± 3.6	0.217 17	0.0560 ± 0.0096
0.034 18	247.4 ± 2.5	0.220 33	0.0242 ± 0.0076
0.034 92	250.0 ± 4.1	0.221 10	0.0342 ± 0.0067
0.036 43	237.0 ± 3.6	0.223 36	0.0320 ± 0.0050
0.037 29	222.3 ± 2.8	0.224 73	0.0197 ± 0.0051
0.037 72	216.9 ± 3.1	0.227 47	0.0162 ± 0.0043
0.040 26	203.8 ± 1.9	0.231 29	0.0338 ± 0.0049
0.043 37	186.4 ± 2.5	0.235 46	0.0271 ± 0.0043
0.045 04	175.2 ± 2.1	0.236 36	0.0290 ± 0.0046
0.045 87	169.8 ± 2.8	0.238 60	0.0325 ± 0.0043
0.046 68	163.9 ± 1.3	0.240 11	0.0401 ± 0.0064
0.049 12	151.0 ± 1.8	0.242 94	0.0376 ± 0.0058
0.054 27	126.4 ± 2.1	0.243 70	0.0318 ± 0.0059
0.056 32	118.0 ± 1.1	0.245 83	0.0426 ± 0.0050
0.058 89	107.7 ± 0.9	0.246 67	0.0441 ± 0.0070
0.064 72	88.1 ± 1.0	0.246 88	0.0521 ± 0.0051
0.066 44	83.9 ± 0.8	0.247 68	0.0485 ± 0.0059
0.069 38	77.0 ± 0.9	0.254 34	0.0846 ± 0.0070
0.075 90	59.3 ± 0.5	0.261 81	0.104 ± 0.007
0.077 72	56.5 ± 0.6	0.262 79	0.0815 ± 0.0083
0.081 12	50.3 ± 0.5	0.264 20	0.0798 ± 0.0072
0.087 92	40.2 ± 0.4	0.265 05	0.0880 ± 0.0090
0.089 08	36.5 ± 0.6	0.268 32	0.113 ± 0.007
0.090 31	37.2 ± 0.8	0.269 19	0.105 ± 0.008
0.093 52	32.2 ± 0.3	0.271 44	0.114 ± 0.006
0.098 45	27.3 ± 0.2	0.278 30	0.127 ± 0.008

$-t$ [(GeV/c)^2]	$d\sigma/dt$ [mb/(GeV/c)^2]	$-t$ [(GeV/c)^2]	$d\sigma/dt$ [mb/(GeV/c)^2]
45 GeV			
0.286 74	0.139 ± 0.011	0.358 98	0.174 ± 0.010
0.294 04	0.165 ± 0.004	0.366 24	0.172 ± 0.005
0.309 93	0.174 ± 0.013	0.384 90	0.169 ± 0.011
0.317 65	0.191 ± 0.005	0.392 55	0.141 ± 0.004
0.334 11	0.164 ± 0.011	0.421 30	0.121 ± 0.005
0.341 21	0.183 ± 0.006	0.450 42	0.0917 ± 0.0063
97 GeV			
0.003 32	773.9 ± 14.9	0.074 53	59.5 ± 0.7
0.003 39	744.1 ± 14.9	0.077 01	55.6 ± 0.6
0.005 68	667.2 ± 6.1	0.079 50	50.4 ± 0.5
0.005 75	663.3 ± 11.1	0.087 74	37.8 ± 0.4
0.006 35	623.5 ± 8.0	0.095 92	27.0 ± 0.2
0.007 08	606.3 ± 6.7	0.097 03	26.7 ± 0.3
0.007 83	614.6 ± 7.6	0.099 86	24.3 ± 0.2
0.008 63	588.0 ± 5.0	0.109 04	17.0 ± 0.2
0.008 73	571.3 ± 8.0	0.109 99	16.2 ± 0.1
0.009 46	568.7 ± 7.2	0.115 74	12.7 ± 0.1
0.010 35	562.5 ± 6.3	0.125 07	8.81 ± 0.11
0.011 00	533.4 ± 5.4	0.131 20	7.13 ± 0.09
0.011 25	536.3 ± 6.1	0.139 26	4.79 ± 0.12
0.011 71	517.7 ± 9.1	0.140 04	4.85 ± 0.07
0.012 22	503.7 ± 5.2	0.147 26	3.38 ± 0.04
0.012 92	500.1 ± 5.2	0.163 26	1.61 ± 0.04
0.014 74	454.6 ± 7.9	0.166 15	1.28 ± 0.03
0.014 88	453.3 ± 7.9	0.174 95	0.781 ± 0.023
0.015 00	465.8 ± 5.0	0.178 74	0.674 ± 0.027
0.015 28	456.5 ± 4.5	0.184 59	0.413 ± 0.012
0.016 41	440.3 ± 3.8	0.191 94	0.267 ± 0.013
0.017 22	428.3 ± 4.7	0.193 95	0.205 ± 0.016
0.019 32	407.2 ± 5.0	0.201 79	0.110 ± 0.011
0.019 61	390.8 ± 4.0	0.204 02	0.0899 ± 0.0055
0.019 93	386.8 ± 6.9	0.208 70	0.0532 ± 0.0067
0.020 10	390.2 ± 6.9	0.216 92	0.0200 ± 0.0034
0.020 59	381.4 ± 4.2	0.222 33	0.0133 ± 0.0023
0.023 17	349.1 ± 4.4	0.225 12	0.0111 ± 0.0023
0.024 54	328.1 ± 3.8	0.233 57	0.0167 ± 0.0034
0.029 58	292.4 ± 3.8	0.233 67	0.0144 ± 0.0034
0.029 92	277.8 ± 3.2	0.240 36	0.0211 ± 0.0034
0.031 13	268.1 ± 3.2	0.249 83	0.0455 ± 0.0044
0.034 66	233.9 ± 2.8	0.255 48	0.0576 ± 0.0067
0.036 77	216.5 ± 3.3	0.257 97	0.0599 ± 0.0044
0.042 41	188.1 ± 2.3	0.267 79	0.0909 ± 0.0055
0.047 10	160.4 ± 2.0	0.278 27	0.112 ± 0.010
0.049 06	141.3 ± 1.6	0.284 40	0.129 ± 0.004
0.050 96	135.7 ± 2.0	0.291 11	0.140 ± 0.008
0.051 98	133.0 ± 1.8	0.296 00	0.152 ± 0.011
0.061 00	96.6 ± 0.9	0.315 43	0.160 ± 0.009
0.070 57	67.8 ± 0.6	0.334 31	0.149 ± 0.009
146 GeV			
0.003 56	757.0 ± 12.1	0.006 62	626.8 ± 7.0
0.004 62	705.0 ± 12.0	0.008 15	595.9 ± 6.2
0.005 25	675.1 ± 7.3	0.008 96	585.5 ± 5.9
0.005 92	659.4 ± 4.5	0.009 08	571.0 ± 8.1
0.006 00	653.0 ± 6.6	0.009 83	562.0 ± 4.5

TABLE I. (*Continued*).

$-t$ [(GeV/c)^2]	$d\sigma/dt$ [mb/(GeV/c)^2]	$-t$ [(GeV/c)^2]	$d\sigma/dt$ [mb/(GeV/c)^2]
	146 GeV		
0.010 74	541.3 ± 3.9	0.099 12	23.6 ± 0.2
0.011 40	526.7 ± 4.7	0.102 82	21.0 ± 0.2
0.011 68	531.5 ± 3.7	0.112 90	13.9 ± 0.1
0.012 16	529.7 ± 8.1	0.119 15	10.9 ± 0.1
0.012 68	505.0 ± 3.2	0.128 74	6.94 ± 0.10
0.013 38	493.8 ± 4.5	0.135 03	5.61 ± 0.08
0.015 46	462.4 ± 3.2	0.151 48	2.52 ± 0.03
0.015 84	457.6 ± 3.3	0.161 49	1.55 ± 0.03
0.017 81	420.3 ± 3.0	0.167 96	1.07 ± 0.03
0.020 01	399.8 ± 4.5	0.170 89	0.891 ± 0.022
0.020 27	388.3 ± 2.4	0.179 92	0.522 ± 0.021
0.020 71	383.3 ± 4.2	0.183 87	0.425 ± 0.022
0.023 96	345.3 ± 4.0	0.189 83	0.260 ± 0.009
0.025 38	328.7 ± 3.4	0.197 36	0.138 ± 0.009
0.025 66	330.4 ± 2.2	0.199 51	0.114 ± 0.012
0.030 56	271.8 ± 3.2	0.209 77	0.0334 ± 0.0052
0.030 89	271.2 ± 2.8	0.214 58	0.0209 ± 0.0042
0.035 76	229.6 ± 2.5	0.228 59	0.0094 ± 0.0020
0.037 97	217.0 ± 2.7	0.231 46	0.0042 ± 0.0020
0.043 74	172.8 ± 2.0	0.240 12	0.0209 ± 0.0031
0.044 86	167.8 ± 1.8	0.240 29	0.0167 ± 0.0042
0.050 60	134.2 ± 1.4	0.247 09	0.0376 ± 0.0042
0.052 52	132.0 ± 1.6	0.256 82	0.0543 ± 0.0052
0.053 75	125.1 ± 1.2	0.262 70	0.0793 ± 0.0073
0.061 12	93.3 ± 1.0	0.265 19	0.0783 ± 0.0052
0.062 80	90.5 ± 1.0	0.274 81	0.105 ± 0.004
0.064 91	84.2 ± 1.0	0.286 10	0.108 ± 0.009
0.071 42	66.6 ± 0.7	0.292 31	0.127 ± 0.005
0.072 72	62.7 ± 0.6	0.299 21	0.144 ± 0.007
0.076 76	55.8 ± 0.7	0.304 32	0.143 ± 0.009
0.079 34	50.4 ± 0.5	0.311 98	0.148 ± 0.005
0.081 91	44.3 ± 0.4	0.324 18	0.144 ± 0.008
0.083 94	41.5 ± 0.4	0.337 47	0.147 ± 0.005
0.088 27	35.9 ± 0.4	0.343 57	0.171 ± 0.007
0.090 37	33.4 ± 0.4	0.363 97	0.147 ± 0.005
0.093 10	29.8 ± 0.3	0.384 51	0.0678 ± 0.0031
	200 GeV		
0.003 82	716.6 ± 7.0	0.029 76	278.7 ± 2.9
0.005 32	652.8 ± 6.3	0.031 08	267.0 ± 2.5
0.006 58	628.9 ± 8.0	0.032 45	252.4 ± 1.6
0.007 08	615.2 ± 5.0	0.035 84	223.8 ± 2.0
0.007 30	620.0 ± 7.2	0.038 56	206.4 ± 2.2
0.009 09	578.7 ± 4.5	0.039 48	202.4 ± 2.5
0.009 34	563.8 ± 5.7	0.041 23	185.0 ± 2.2
0.011 64	518.1 ± 5.3	0.042 48	178.4 ± 1.7
0.012 48	507.5 ± 3.7	0.045 43	161.8 ± 1.3
0.013 16	504.0 ± 4.7	0.050 83	136.1 ± 2.0
0.014 17	476.6 ± 4.2	0.052 65	125.8 ± 1.0
0.014 91	467.2 ± 4.7	0.055 40	114.3 ± 1.2
0.015 85	457.5 ± 4.2	0.061 45	93.4 ± 1.2
0.016 77	434.4 ± 2.5	0.063 42	86.8 ± 0.9
0.017 94	418.8 ± 3.3	0.066 45	76.7 ± 0.7
0.020 36	390.9 ± 4.2	0.074 16	58.3 ± 0.5
0.021 24	374.9 ± 1.9	0.078 51	49.7 ± 0.4
0.024 43	337.1 ± 2.3	0.083 15	41.3 ± 0.5
0.025 44	325.4 ± 3.0	0.086 93	36.0 ± 0.3
0.026 84	309.5 ± 2.7	0.091 58	30.5 ± 0.2
0.028 35	295.3 ± 2.7	0.096 59	25.1 ± 0.3
	200 GeV		
0.100 45	21.6 ± 0.1	0.240 52	0.0217 ± 0.0036
0.105 65	17.5 ± 0.1	0.242 31	0.0317 ± 0.0036
0.111 04	14.4 ± 0.1	0.244 98	0.0323 ± 0.0036
0.113 96	12.7 ± 0.1	0.249 33	0.0502 ± 0.0061
0.120 74	9.48 ± 0.11	0.253 50	0.0543 ± 0.0046
0.126 49	7.52 ± 0.09	0.257 35	0.0666 ± 0.0061
0.136 85	4.73 ± 0.09	0.261 96	0.0756 ± 0.0046
0.142 96	3.56 ± 0.06	0.266 47	0.0877 ± 0.0052
0.149 07	2.63 ± 0.03	0.275 92	0.102 ± 0.003
0.153 96	2.32 ± 0.05	0.288 62	0.128 ± 0.007
0.166 11	1.12 ± 0.01	0.301 69	0.138 ± 0.003
0.184 20	0.378 ± 0.009	0.314 96	0.147 ± 0.007
0.198 45	0.108 ± 0.012	0.331 24	0.149 ± 0.003
0.202 36	0.0727 ± 0.0085	0.358 01	0.139 ± 0.003
0.205 12	0.0648 ± 0.0064	0.384 82	0.121 ± 0.004
0.206 46	0.0410 ± 0.0064	0.413 19	0.102 ± 0.003
0.213 75	0.0200 ± 0.0031	0.443 97	0.0722 ± 0.0031
0.217 81	0.0076 ± 0.0021	0.476 32	0.0519 ± 0.0032
0.225 99	0.0151 ± 0.0051	0.509 00	0.0298 ± 0.0032
0.227 39	0.0110 ± 0.0045		
	259 GeV		
0.003 88	729.0 ± 8.5	0.088 72	33.9 ± 0.4
0.007 19	629.6 ± 6.3	0.092 58	29.6 ± 0.3
0.009 22	578.4 ± 5.0	0.097 58	24.9 ± 0.3
0.009 46	569.3 ± 7.0	0.100 31	22.2 ± 0.2
0.012 77	512.6 ± 6.6	0.102 74	19.6 ± 0.2
0.013 33	502.6 ± 5.8	0.106 73	17.2 ± 0.1
0.014 35	488.2 ± 5.4	0.112 18	13.9 ± 0.1
0.015 09	465.4 ± 5.9	0.115 09	12.2 ± 0.1
0.016 05	461.4 ± 4.7	0.121 96	9.16 ± 0.12
0.016 84	439.5 ± 4.0	0.127 77	7.19 ± 0.09
0.017 17	438.8 ± 4.2	0.138 22	4.47 ± 0.08
0.020 62	391.5 ± 4.3	0.144 40	3.35 ± 0.06
0.021 12	384.7 ± 4.3	0.151 23	2.32 ± 0.04
0.021 52	377.5 ± 2.8	0.162 04	1.41 ± 0.04
0.024 52	336.8 ± 3.3	0.165 54	1.13 ± 0.03
0.025 74	322.3 ± 3.5	0.168 05	1.000 ± 0.030
0.027 16	309.2 ± 3.2	0.180 71	0.430 ± 0.021
0.028 67	294.0 ± 3.3	0.186 57	0.293 ± 0.009
0.030 09	286.6 ± 3.0	0.207 08	0.0380 ± 0.0053
0.031 44	267.2 ± 3.1	0.208 45	0.0199 ± 0.0060
0.032 79	254.3 ± 1.9	0.215 84	0.0107 ± 0.0033
0.036 23	225.1 ± 2.4	0.219 89	0.0073 ± 0.0026
0.038 99	208.2 ± 2.3	0.226 45	0.0060 ± 0.0026
0.039 93	198.6 ± 2.1	0.229 56	0.0119 ± 0.0040
0.042 93	179.7 ± 2.0	0.230 60	0.0099 ± 0.0026
0.045 89	161.3 ± 1.4	0.242 86	0.0478 ± 0.0066
0.049 43	139.7 ± 1.9	0.244 60	0.0341 ± 0.0040
0.051 38	134.5 ± 1.7	0.247 15	0.0518 ± 0.0039
0.053 45	122.5 ± 1.5	0.251 72	0.0601 ± 0.0060
0.055 99	110.9 ± 1.2	0.255 90	0.0707 ± 0.0046
0.062 08	92.6 ± 1.3	0.259 85	0.0741 ± 0.0112
0.064 10	82.0 ± 0.7	0.264 29	0.0890 ± 0.0078
0.067 15	75.8 ± 0.7	0.269 00	0.0946 ± 0.0054
0.073 80	59.8 ± 0.7	0.278 84	0.115 ± 0.003
0.079 32	48.1 ± 0.4	0.291 34	0.124 ± 0.010
0.084 03	41.1 ± 0.5	0.300 21	0.150 ± 0.005
0.086 55	36.9 ± 0.4	0.308 22	0.152 ± 0.004

TABLE I. (*Continued*).

$-t$ $[(\mathrm{GeV}/c)^2]$	$d\sigma/dt$ $[\mathrm{mb}/(\mathrm{GeV}/c)^2]$	$-t$ $[(\mathrm{GeV}/c)^2]$	$d\sigma/dt$ $[\mathrm{mb}/(\mathrm{GeV}/c)^2]$
	259 GeV		
0.31794	0.143 ± 0.010	0.41639	0.0909 ± 0.0029
0.32707	0.128 ± 0.009	0.44767	0.0598 ± 0.0026
0.33551	0.152 ± 0.004	0.48049	0.0393 ± 0.0025
0.36113	0.138 ± 0.003	0.51373	0.0340 ± 0.0033
0.38759	0.115 ± 0.003		
	301 GeV		
0.00385	717.8 ± 9.5	0.08943	31.3 ± 0.5
0.00666	636.9 ± 8.0	0.09271	28.7 ± 0.2
0.00715	626.4 ± 7.1	0.09781	23.4 ± 0.2
0.00738	596.0 ± 7.1	0.10185	19.7 ± 0.1
0.00863	584.4 ± 6.1	0.10701	16.4 ± 0.2
0.00920	567.1 ± 4.6	0.11244	13.1 ± 0.1
0.00944	560.7 ± 5.6	0.11534	11.6 ± 0.1
0.01176	523.2 ± 5.5	0.12224	8.49 ± 0.10
0.01243	513.9 ± 6.1	0.12810	6.68 ± 0.08
0.01433	479.4 ± 4.3	0.13856	4.02 ± 0.08
0.01507	464.7 ± 4.7	0.14478	3.15 ± 0.06
0.01605	448.5 ± 4.3	0.15102	2.24 ± 0.03
0.01696	434.6 ± 2.6	0.15586	1.86 ± 0.05
0.01815	419.4 ± 3.3	0.16781	0.930 ± 0.013
0.02062	387.6 ± 4.4	0.18660	0.274 ± 0.008
0.02147	374.1 ± 1.9	0.20097	0.0789 ± 0.0090
0.02473	328.4 ± 2.3	0.20484	0.0581 ± 0.0080
0.02576	317.9 ± 3.0	0.20764	0.0529 ± 0.0047
0.02716	300.9 ± 2.7	0.20900	0.0351 ± 0.0070
0.02869	293.0 ± 2.7	0.21646	0.0039 ± 0.0024
0.03010	278.1 ± 3.1	0.22049	0.0024 ± 0.0019
0.03148	261.2 ± 2.5	0.22713	0.0119 ± 0.0033
0.03263	247.7 ± 2.4	0.22876	0.0085 ± 0.0047
0.03626	220.5 ± 2.1	0.23020	0.0127 ± 0.0047
0.03902	201.9 ± 2.3	0.23124	0.0123 ± 0.0033
0.04172	186.6 ± 2.3	0.24358	0.0378 ± 0.0048
0.04298	174.2 ± 1.7	0.24528	0.0454 ± 0.0043
0.04595	157.2 ± 1.1	0.24784	0.0464 ± 0.0039
0.04951	138.5 ± 2.0	0.25242	0.0647 ± 0.0075
0.05144	128.1 ± 1.8	0.25662	0.0761 ± 0.0057
0.05328	122.5 ± 1.0	0.26062	0.0743 ± 0.0071
0.05607	109.8 ± 1.1	0.26502	0.0805 ± 0.0058
0.06217	88.2 ± 1.1	0.26977	0.0915 ± 0.0058
0.06413	82.0 ± 0.8	0.27891	0.110 ± 0.003
0.06727	72.4 ± 0.6	0.29217	0.130 ± 0.006
0.07509	55.2 ± 0.4	0.30544	0.142 ± 0.003
0.07948	46.8 ± 0.4	0.31887	0.140 ± 0.007
0.08421	39.2 ± 0.4	0.33514	0.139 ± 0.003
0.08671	35.0 ± 0.3	0.36251	0.122 ± 0.003

$-t$ $[(\mathrm{GeV}/c)^2]$	$d\sigma/dt$ $[\mathrm{mb}/(\mathrm{GeV}/c)^2]$	$-t$ $[(\mathrm{GeV}/c)^2]$	$d\sigma/dt$ $[\mathrm{mb}/(\mathrm{GeV}/c)^2]$
	301 GeV		
0.38898	0.0980 ± 0.0032	0.48243	0.0428 ± 0.0027
0.41760	0.0822 ± 0.0028	0.51534	0.0332 ± 0.0034
0.44944	0.0551 ± 0.0025		
	393 GeV		
0.00385	720.9 ± 10.1	0.10392	18.4 ± 0.4
0.00718	639.8 ± 7.4	0.10746	16.0 ± 0.1
0.00922	597.7 ± 6.0	0.11293	12.9 ± 0.2
0.00948	591.6 ± 8.7	0.11591	11.4 ± 0.1
0.01180	540.1 ± 6.7	0.12291	8.56 ± 0.19
0.01278	511.0 ± 7.7	0.12867	6.68 ± 0.09
0.01335	512.1 ± 7.0	0.13920	4.10 ± 0.09
0.01439	495.9 ± 6.5	0.14543	3.14 ± 0.07
0.01513	490.9 ± 7.2	0.15118	2.16 ± 0.04
0.01609	466.3 ± 5.7	0.16322	1.21 ± 0.05
0.01702	451.2 ± 3.4	0.16920	0.809 ± 0.018
0.01804	437.6 ± 5.5	0.18205	0.415 ± 0.024
0.02067	399.1 ± 5.1	0.18805	0.247 ± 0.009
0.02160	377.2 ± 2.6	0.20191	0.0625 ± 0.0118
0.02483	342.9 ± 3.0	0.20589	0.0441 ± 0.0085
0.02584	328.5 ± 4.1	0.20869	0.0284 ± 0.0088
0.02727	315.0 ± 3.7	0.21004	0.0100 ± 0.0079
0.03023	285.3 ± 3.5	0.21750	0.0073 ± 0.0060
0.03158	267.4 ± 3.5	0.22162	0.0092 ± 0.0053
0.03295	253.7 ± 2.2	0.22821	0.0193 ± 0.0053
0.03641	225.4 ± 2.7	0.22994	0.0125 ± 0.0066
0.03917	208.5 ± 2.7	0.23134	0.0183 ± 0.0081
0.04190	186.2 ± 2.1	0.23242	0.0132 ± 0.0046
0.04317	177.6 ± 2.3	0.24475	0.0384 ± 0.0074
0.04614	160.1 ± 1.5	0.24654	0.0542 ± 0.0053
0.04970	138.6 ± 2.2	0.24913	0.0539 ± 0.0061
0.05167	128.1 ± 1.9	0.25369	0.0808 ± 0.0079
0.05339	121.8 ± 1.1	0.25795	0.0824 ± 0.0067
0.05631	113.1 ± 1.4	0.26189	0.0985 ± 0.0141
0.06247	89.6 ± 1.5	0.26641	0.0957 ± 0.0107
0.06475	81.9 ± 1.0	0.27861	0.116 ± 0.003
0.06757	75.2 ± 0.8	0.29370	0.121 ± 0.012
0.07428	58.1 ± 0.8	0.30707	0.142 ± 0.004
0.07642	52.6 ± 0.7	0.32051	0.142 ± 0.013
0.07983	46.0 ± 0.5	0.33723	0.141 ± 0.004
0.08456	40.1 ± 0.5	0.36412	0.127 ± 0.004
0.08713	35.6 ± 0.4	0.39096	0.101 ± 0.004
0.08933	32.4 ± 0.5	0.42034	0.0787 ± 0.0033
0.09313	28.2 ± 0.3	0.45154	0.0561 ± 0.0030
0.09823	23.0 ± 0.3	0.48476	0.0382 ± 0.0029
0.10101	20.7 ± 0.3	0.51808	0.0268 ± 0.0034

$\mathrm{g/cm^2}$ and a jet width (rms) of ±3 mm. The gas-jet pulse length is 100 msec and occurs at two energies during the accelerator ramp cycle. During the "live time" of the gas jet the value of the actual beam energy is written into the computer every 40 msec. The variation of primary energy over the jet pulse length is ±8 GeV or less depending on the accelerator rate of rise.

Helium is injected into a 250-l buffer volume, and 90% of the gas is removed by a 5000-l/sec diffusion pump. The remainder is removed from the accelerator vacuum chamber by 8 diffusion pumps spaced at 5-m intervals upstream and downstream from the target. These pumps constitute a differential pumping system and reduce the helium partial pressure to 10^{-9} mm Hg beyond the last upstream and downstream pumps.

The target is viewed at near 90° by sets of

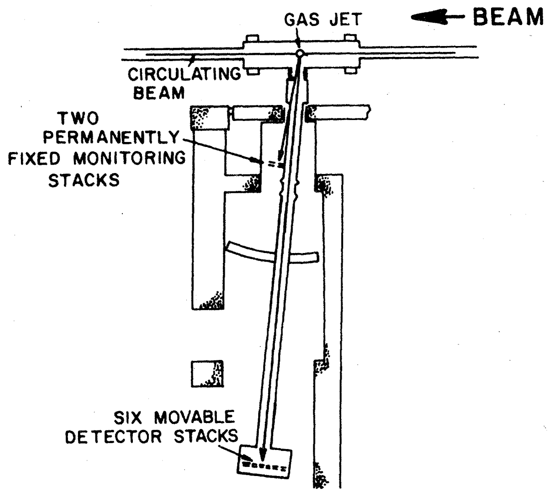

FIG. 1. Schematic representation of the apparatus.

stacks of solid-state detectors. Each stack consists of two silicon detectors with typical dimensions of 5×30 mm^2. The thickness of the front detectors ranges from 15 to 250 μm and of the back detectors from 200 to 1500 μm. The detectors have a noise of 50 keV and energy resolutions of 50–150 keV. The six movable stacks are installed at 7.2 m from the target inside of the vacuum chamber, which, together with the "ion-guide" connecting it with the target chamber, forms a remotely movable arm. The range of laboratory angles covered by the detectors is 84.5°–89.7° (relative to the beam direction). The relative position of the detector arm is measured with accuracy ± 0.02 mrad; the relative angles between stacks are known with accuracy ± 0.025 mrad and remain constant for the whole experiment.

The 7.2-m distance from the target and the detector dimensions yields a geometric resolution of $\Delta\theta = \pm 0.7$ mrad. The resulting kinetic-energy uncertainty $\Delta T/T = 2\,\Delta\theta/\theta$, where θ is the recoil angle with respect to 90°, is good enough to provide separation between the elastic and inelastic reactions. Two additional permanently fixed stacks are used to monitor the jet-beam interaction rate. During readout of a stack, the inputs to all other stacks are inhibited. Thus, all channels have the same dead-time percentage (3%). A typical counting rate is about 1000 events per beam spill distributed over eight stacks.

The $|t|$ interval studied is $0.003 \leq |t| \leq 0.52$ $(\mathrm{GeV}/c)^2$ corresponding to recoil angles of $6 < \theta < 96$ mrad and ranges of $2 < R < 1800$ μm silicon. The multiple scattering of the outgoing recoil particle in the target gas is negligible except at the smallest $|t|$ values. In the worst case, at $|t| \simeq 0.003$ $(\mathrm{GeV}/c)^2$, the multiple scattering mainly affects the energy resolution, but the corrections to the cross section are smaller than 1%.

The detectors are calibrated against a $^{234}_{90}$Th α-particle source. When compared with survey measurements, the absolute angles determined from the elastic peak show an offset difference of 0.3 mrad; this is consistent with the absolute angular uncertainty estimated to be less than ± 0.2 mrad. The magnetic-field action on the recoils is reduced by shielding to ≤ 0.03 G in order to minimize angular errors at low $|t|$. At $|t| = 0.003$ $(\mathrm{GeV}/c)^2$ the remaining field can cause at most an angular change of ≤ 0.12 mrad.

The first step in the analysis is to separate coherent ^{4}He recoils from H, D, T, ^{3}He. The energies in MeV deposited in the detector sandwiches are sorted into 256×256 plots of the front detector T_F versus the back detector T_B. The mass of a ^{4}He particle stopping in the back element is deduced from the known range-energy relation and is given by the empirical formula

$$m = m_p \left[\frac{\alpha}{d_F} \left| (T_F + T_B)^{\beta} - T_B{}^{\beta} \right| \right]^{1/(\beta-1)} Z^{-2}, \qquad (1)$$

where $\alpha = 13.3$, $\beta = 1.73$, and d_F is the thickness of the front detector in μm. In Figs. 2(a) and 2(b) we plot the recoil mass distribution for $t = -0.149$ and -0.450 $(\mathrm{GeV}/c)^2$, respectively. The ^{4}He, ^{3}He mass separation is excellent at these $|t|$ values.

For the separated ^{4}He recoils the momentum spectra are obtained and described by a formula which contains Gaussian plus polynomial back-

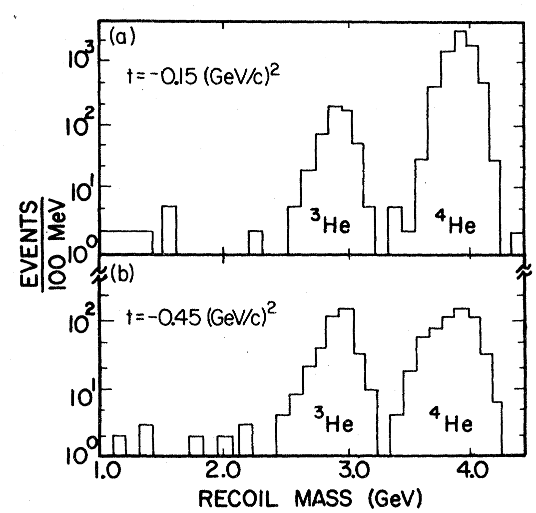

FIG. 2. Mass distribution obtained from the two-dimensional plot using relation (1). The peaks corresponding to isotopes ^{3}He, ^{4}He are shown.

ground terms. The number of elastic-scattering events is calculated as the sum over the peak within the limit $\pm 4\sigma$. The number of background events under the elastic peak is usually 1–3 % except for the region of the diffraction minimum. In the dip region, $t \simeq -0.22$ $(\mathrm{GeV}/c)^2$, the p^4He elastic cross section drops 5 orders of magnitude, and the systematic uncertainty is about $\pm 50\%$ due to inelastic background subtraction.

The results from an analysis of the inelastic p^4He reactions are presented in the accompanying paper[13] on coherent proton diffraction dissociation of helium from 45 to 400 GeV.

III. ABSOLUTE NORMALIZATION

The ratios of the proton-helium to the proton-proton differential cross section have been obtained from auxiliary measurements using a hydrogen/helium mixture as a target. Three of the movable stacks and one of the two fixed monitoring stacks are used to observe pp elastic scattering. The other half of the detector stacks are used to see p^4He elastic scattering.

The absolute value of $d\sigma_{p\mathrm{He}}/d\omega$ is calculated from the relation

$$\frac{d\sigma_{p\mathrm{He}}}{d\omega} = \frac{n_{\mathrm{He}}}{n_p}\,\frac{\Delta\omega_p}{\Delta\omega_{\mathrm{He}}}\,\frac{k_p}{k_{\mathrm{He}}}\,\frac{d\sigma_{pp}}{d\omega}\,, \tag{2}$$

where n is the number of elastic-scattering events, $\Delta\omega$ is the solid angle of the stack, k is the atomic concentration of gas and $d\sigma_{pp}/d\omega$ is the known differential cross section for elastic pp scattering. The auxiliary experiment has been done at nine energies: 49, 66, 90, 161, 200, 258, 280, 301, and 393 GeV in a range $0.001 < |t| < 0.02$ for pp and $0.007 < |t| < 0.11$ $(\mathrm{GeV}/c)^2$ for p^4He. Since this is a new technique, there are a number of concerns we have about possible systematic errors. The mixture ratio could change as the gas emerged from the gas-jet nozzle. To examine this possibility we looked for a possible time structure in the ratio n_{He}/n_p within the 100-msec spill. We also compared the shape and width of the hydrogen and helium jets obtained by unfolding them from the elastic pulse-height distribution

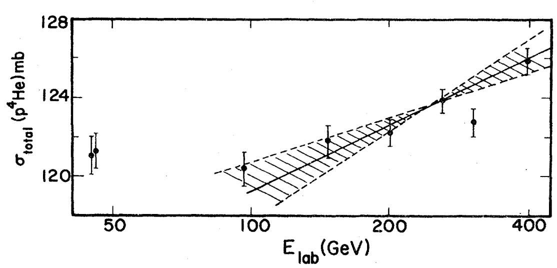

FIG. 3. Total cross section for p^4He interactions. The straight line is calculated according to the geometric-scaling relation, σ_{tot} proportional to b, the slope parameter (see Table IV). The dashed area is the 1-standard-deviation corridor uncertainty.

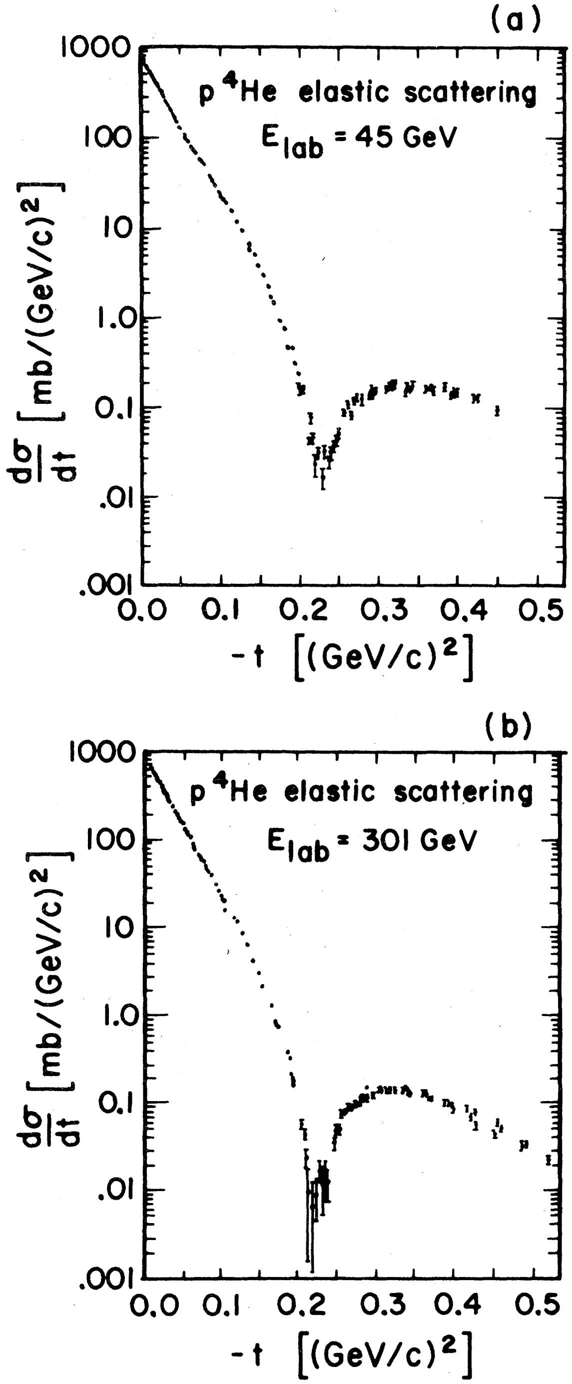

FIG. 4. Examples of the differential cross section of p^4He elastic scattering: (a) E_{lab}=45 GeV, (b) E_{lab}=301 GeV.

TABLE II. Systematic errors in $d\sigma/dt$.

	Dependent on t	Dependent on E_{lab}	Lowest $\|t\|$ Lowest E_{lab} (%)	Lowest $\|t\|$ Highest E_{lab} (%)	Highest $\|t\|$ Lowest E_{lab} (%)	Highest $\|t\|$ Highest E_{lab} (%)	Dip region $t_{min} \simeq -0.24$ $(GeV/c)^2$ Lowest E_{lab} (%)	Dip region $t_{min} \simeq -0.22$ $(GeV/c)^2$ Highest E_{lab} (%)
Collimator area	No	No	0.5	0.5	0.5	0.5	0.5	0.5
Monitor (statistical error)	No	No	1.0	1.0	1.0	1.0	1.0	1.0
Absolute angular scale uncertainty ±0.2 mrad	Yes	No[a]	0.3	0.3	0.3	0.3	2.0	2.0
Magnetic field	Yes	No	0.1	0.1	0	0	0	0
Background (residual gas)	No	No	0.3	0.3	0.3	0.3	0.3	0.3
Inelastic background	Yes	Yes	0.0	0.0	0.0	3.0	0.0	50.0
Absolute normalization	No	No	4.8	4.8	4.8	4.8	4.8	4.8

[a] Systematic error depends on the depth of the dip region.

TABLE III. Total elastic cross section, and position and height of the second maximum. The systematic error in $\sigma_{tot\,el}$ is ± 1.24 mb.

E_{lab} (GeV)	$\sigma_{tot\,el}$ (mb)	$-t_{sec\,max}$ $[(GeV/c)^2]$	$(d\sigma/dt)_{sec\,max}$ $[mb/(GeV/c)^2]$
45	23.09 ± 0.23	0.319	0.190 ± 0.015
46	22.80 ± 0.23	0.318	0.184 ± 0.016
97	22.26 ± 0.22	0.321	0.160 ± 0.010
146	22.37 ± 0.22	0.328	0.167 ± 0.010
200	22.18 ± 0.22	0.324	0.166 ± 0.010
259	22.54 ± 0.23	0.326	0.150 ± 0.016
301	22.11 ± 0.22	0.327	0.153 ± 0.012
393	22.93 ± 0.23	0.333	0.147 ± 0.010

using elastic kinematics. No differences were seen.

To look for longer-term time variation, we plotted the ratio of the number of detected elastic events for pp and $p\,^4$He collisions from run to run for the two fixed stacks. This ratio remains constant during the data-collection time of about 30 h (16 independent runs). We conclude that the ratio of luminosities of the partial targets (hydrogen and helium) is independent of time.

An additional check of this technique has been performed using a hydrogen-deuterium mixture as a target. In this case both differential cross sections are known. From the measured ratio n_p/n_d we deduce the absolute value of the differential pd cross section and, using the optical theorem, calculate the total cross section for pd interactions: $\sigma_{tot}(pd) = 73.24 \pm 0.47$ mb at $E = 49$ GeV and 74.61 ± 0.47 mb at $E = 259$ GeV. This is in good agreement with the data by Carrol *et al.*[14]

The auxiliary experiment with a hydrogen-helium mixture has been done at a limited number of angular points. The data obtained are used only for absolute normalization of the relative cross sections measured in the course of the main experiment.

Normalization is done as follows. Using a starting value for the total cross section, fits are made to the data of the main experiment by techniques described in Sec. IV. Once parameters describing the shape of the differential cross section are found, the mixture data is used to find the correct normalization for the main experiment. With normalization now fixed, a new fit is done to the main experiment data and iteration continued until the parameters are stable. Since the energy of the primary beam in these two sets of measurement is slightly different, corresponding interpolation is done.

Results are shown in Fig. 3. The errors shown are only statistical. The systematic error is

TABLE IV. The parameters of Bethe's formula Eqs. (3)–(5) describing the differential cross section for elastic p^4He scattering in an interval $0.003 \le t \le 0.11$ $(\mathrm{GeV}/c)^2$.

E_{lab} (GeV)	$\sigma_{\mathrm{tot}}^{p\mathrm{He}}$ (mb)	ρ	b $[(\mathrm{GeV}/c)^{-2}]$	c $[(\mathrm{GeV}/c)^{-4}]$	χ^2/No. of points
45	121.1 ± 1.0	-0.056 ± 0.030	31.4 ± 0.4	-25 ± 3	81/72
46	121.4 ± 0.9	-0.012 ± 0.032	32.0 ± 0.4	-19 ± 3	56/60
97	120.3 ± 0.9	-0.053 ± 0.026	32.1 ± 0.3	-23 ± 3	98/57
146	121.8 ± 0.8	-0.024 ± 0.024	32.5 ± 0.3	-25 ± 3	100/71
200	122.3 ± 0.7	$+0.041 \pm 0.023$	32.9 ± 0.3	-25 ± 2	59/73
259	123.9 ± 0.7	$+0.046 \pm 0.031$	33.5 ± 0.3	-21 ± 3	55/60
301	122.8 ± 0.7	$+0.042 \pm 0.030$	33.4 ± 0.3	-24 ± 3	58/65
393	125.9 ± 0.6	$+0.102 \pm 0.035$	34.2 ± 0.4	-21 ± 3	54/64
Systematic error	$\pm 2.4\%$	± 0.05	± 0.16	± 0.7	

hard to estimate given some of the problems discussed above. The hydrogen/helium mixture is 48.33%/51.56%. This ratio is known with a precision of ±4%. The corresponding uncertainty in $\sigma_{\mathrm{tot}}^{p\mathrm{He}}$ is ±2.5 mb. There are two additional sources of systematic uncertainty in $\sigma_{\mathrm{tot}}^{p\mathrm{He}}$. Background subtraction in the mixture experiment contributes an uncertainty of ±1.5 mb. Extrapolation to the optical point depends on the model used. If, e.g., we use the parametrization of Schiz *et al.*[15] instead of the pp parametrization we have used, this lowers $\sigma_{\mathrm{tot}}^{p\mathrm{He}}$ by about 1.7 mb. The total systematic error in $\sigma_{\mathrm{tot}}^{p\mathrm{He}}$ is then estimated as ±3 mb.

After this paper was written preliminary results from a new CERN experiment became known to us.[16] Since they use an external beam and a conventional target they, in principle, can determine their normalization more accurately. Of course, to obtain $\sigma_{\mathrm{tot}}^{p\mathrm{He}}$ one must assume a shape for the differential cross section and extrapolate to $t=0$. Their preliminary total cross section is 8–9 mb higher than ours; their quoted total error is ±0.8 mb. The amusing part is that these preliminary CERN results agree with our preliminary results, presented at the Tokyo conference.[17] In that case we normalized using the differential cross section in the Coulomb interference region. Although it gave statistical accuracy comparable to this paper, we feel the mixture technique is inherently more reliable than the Coulomb technique because in that case the value obtained depends critically on the cross-section shape used.

The main virtue of our measurements lies in the wide range of s and t covered with one experimental setup. It is a simple matter at a later date, if necessary, to renormalize the data in Table I and refit to any desired model.

IV. DIFFERENTIAL CROSS SECTIONS

The differential cross sections for $p\,^4$He elastic scattering are given in Table I. The errors listed are statistical only. Examples of the differential cross section $d\sigma/dt$ are shown in Figs. 4(a) and 4(b). The general characteristics of the data are a differential cross section which drops 4–5 orders of magnitude to a first dip at $|t| \simeq 0.22$ $(\mathrm{GeV}/c)^2$ and a subsequent rise to a secondary maximum at $|t| \simeq 0.33$ $(\mathrm{GeV}/c)^2$.

The sources of systematic errors and their

TABLE V. The same as in Table IV but with $c=-22$ $(\mathrm{GeV}/c)^{-4}$ a fixed parameter.

E_{lab} (GeV)	$\sigma_{\mathrm{tot}}^{p\mathrm{He}}$ (mb)	ρ	b $[(\mathrm{GeV}/c)^{-2}]$	χ^2/No. of points
45	121.33 ± 0.59	-0.068 ± 0.032	31.71 ± 0.10	82/72
46	120.32 ± 0.60	-0.063 ± 0.025	31.55 ± 0.11	56/60
97	120.49 ± 0.56	-0.065 ± 0.021	32.32 ± 0.09	110/57
146	121.97 ± 0.43	-0.036 ± 0.018	32.74 ± 0.08	101/71
200	122.80 ± 0.29	-0.035 ± 0.017	33.34 ± 0.08	62/73
259	123.62 ± 0.37	$+0.010 \pm 0.024$	33.39 ± 0.09	56/60
301	123.22 ± 0.31	$+0.038 \pm 0.022$	33.71 ± 0.08	62/65
393	125.78 ± 0.31	$+0.067 \pm 0.027$	34.07 ± 0.10	54/64

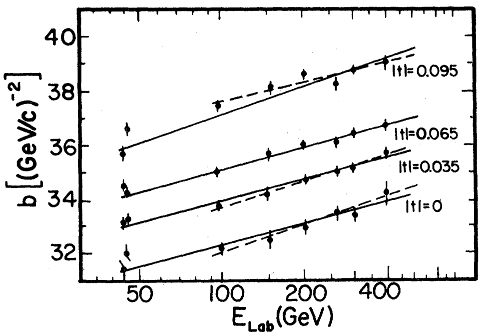

FIG. 5. Average slope parameter of the diffraction peak of p^4He elastic scattering at different t intervals (values from Table VI). The solid lines are fits over the entire energy range. The dashed lines correspond to the fit for energies $E \geq 100$ GeV.

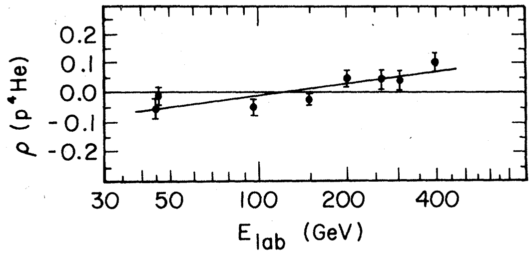

FIG. 6. $\rho = \mathrm{Re} f_n / \mathrm{Im} f_n\ (t=0)$ for $p\,^4$He elastic scattering. The values are from Table IV. The straight-line fit shows the parametrization listed in Table VII.

variation with E_{lab} and t are listed in Table II. These systematic errors are errors on the individual data points; an additional error in the overall normalization must be added. The statistical error of absolute normalization is ±0.7%, the systematic uncertainty is ±4.8%, as explained above. Thus the total error in absolute normalization of the differential cross sections given in Table I is ±4.8%.

Table III lists values of the total elastic $p\,^4$He cross sections. They are obtained by integration of the differential cross section in the t range $0 \leq |t| \leq 0.5$ (GeV/c)^2 after Coulomb and Coulomb-nuclear interference effects are subtracted.

Another general characteristic of the differential cross section is the position and the magnitude of the second maximum. They are given in Table III as well.

V. SMALL-t REGION

The results for the $p\,^4$He elastic cross section, listed in Table I, are described in the range $0.003 \leq |t| \leq 0.11$ (GeV/c)^2 by the Bethe interference formula[18]

$$\frac{d\sigma}{dt} = |f_C e^{i\Phi} + f_n|^2 , \tag{3}$$

where the Coulomb-scattering amplitude takes the form

$$f_C = \frac{4\alpha\hbar\sqrt{\pi}}{t} G_p(t) G_{\mathrm{He}}(t) . \tag{4}$$

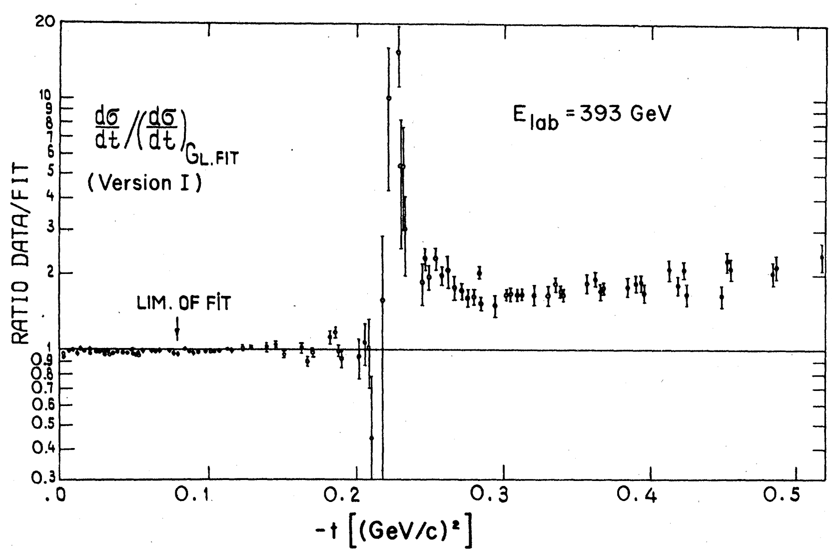

FIG. 7. The elastic differential $p\,^4$He cross section at 393 GeV. The solid line is the Glauber-model prediction; the simplest form of the elementary amplitude and one-particle density has been used (version I in the text). The Coulomb effect for $-t < 0.03$ (GeV/c)^2 is extracted. The data fit is over the range $0.003 \leq |t| \leq 0.07$ (GeV/c)^2. The data is plotted as a ratio of the differential elastic cross section to that of the Glauber-model prediction.

TABLE VI. Average slope parameter in $(\mathrm{GeV}/c)^{-2}$ for three different t intervals.

E_{lab} (GeV)	$0.003<\|t\|<0.07$ $(\mathrm{GeV}/c)^2$ $b_{\|t\|=0.035}$	χ^2/DF	$0.03<\|t\|<0.1$ $(\mathrm{GeV}/c)^2$ $b_{\|t\|=0.065}$	χ^2/DF	$0.06<\|t\|<0.13$ $(\mathrm{GeV}/c)^2$ $b_{\|t\|=0.095}$	χ^2/DF
45	33.13 ± 0.12	60/55	34.48 ± 0.14	33/26	35.63 ± 0.28	33/20
46	33.23 ± 0.13	40/47	34.24 ± 0.15	17/21	36.59 ± 0.25	21/13
97	33.55 ± 0.13	75/40	34.98 ± 0.13	41/17	37.35 ± 0.17	24/15
146	34.18 ± 0.10	61/52	35.60 ± 0.10	58/20	38.16 ± 0.14	61/22
200	34.68 ± 0.09	44/52	36.06 ± 0.09	19/30	38.57 ± 0.13	15/24
259	35.06 ± 0.10	35/42	36.11 ± 0.11	32/27	38.28 ± 0.14	31/27
301	35.16 ± 0.09	39/46	36.43 ± 0.10	30/29	38.87 ± 0.13	28/27
393	35.66 ± 0.12	35/44	36.75 ± 0.12	30/30	39.09 ± 0.17	13/21

Here α is the fine-structure constant, $\phi=4\alpha\ln(1.06\hbar/R\sqrt{|t|})$ is the Coulomb phase, $R=\sqrt{2/3}\langle R_{\mathrm{He}}{}^2\rangle^{1/2}$ is the ^{4}He electromagnetic radius[5,6] ($R_{\mathrm{He}}=1.67$ fm) derived from $e\,^4$He scattering, $G_p(t)=(1-t/0.71)^{-2}$ is the proton electromagnetic form factor, and $G_{\mathrm{He}}(t)=[1-(2.56t)^6]\times e^{11.70t}$ is the ^{4}He electromagnetic form factor.[5,6] The nuclear-scattering amplitude takes the form

$$f_n=\frac{\sigma_{\mathrm{tot}}^{p\mathrm{He}}}{4\hbar\sqrt{\pi}}(i+\rho)e^{(bt+ct^2)/2}\,, \qquad (5)$$

where $\sigma_{\mathrm{tot}}^{p\mathrm{He}}$ is the total proton-helium cross section, $\rho=\mathrm{Re}f_n/\mathrm{Im}f_n|_{t=0}$ is the ratio of the real to the imaginary part of the forward-scattering amplitude, and b,c are the linear and quadratic slope parameters.

The results of the fit in the range $0.003<|t|<0.11$ $(\mathrm{GeV}/c)^2$ are listed in Table IV. The fitted parameters are $\sigma_{\mathrm{tot}}^{p\mathrm{He}}$ ρ, b, and c. The values given for $\sigma_{\mathrm{tot}}^{p\mathrm{He}}$ in Table IV are directly related to the normalization obtained from the mixture analysis. In Fig. 3 we show the Table IV proton-helium total cross sections at 45, 46, 97, 146, 200, 259, 301, and 393 GeV. Since the quadratic slope parameter $c\simeq22$ $(\mathrm{GeV}/c)^{-4}$ is energy independent within errors, an alternate fit with c fixed is listed in Table V.

Table VI presents the average slope parameter in different t intervals $0.003<|t|<0.007$ $(\mathrm{GeV}/c)^2$, $0.03<|t|<0.1$ $(\mathrm{GeV}/c)^2$, and $0.06<|t|<0.13$ $(\mathrm{GeV}/c)^2$ calculated as $b_{t=t_0}=b+2ct_0$, where b and c have been fitted in each interval. Figure 5 shows the slope parameter b as listed in Table VI. The rate of shrinkage weakly depends on t; for energies $E>100$ GeV, the rate of shrinkage is t independent (see dashed lines on Fig. 5).

Finally, to complete our analysis using the Bethe formula, the s dependence of the b, $\sigma_{\mathrm{tot}}^{p\mathrm{He}}$, and ρ values given in Table V has been parametrized in the form $P_i=A_i+B_i\ln(s_{p\mathrm{He}}/s_0)$, with $s_0=1$ GeV^2. These results are given in Table VII. The energy dependence of ρ is plotted in Fig. 6.

The parameter $b(s,t)$ of the $p\,^4$He scattering amplitude obtained shows a rate of shrinkage of the $p\,^4$He diffraction cone $b_1(t)=(\partial/\partial\ln s)b(s,t)$ more than twice as large as that for pp scattering.[19] This effect is in qualitative agreement with the expectation based on the Glauber model provided the screening correction is energy dependent.[20] The other consequence of this model is the increase of the rate of shrinkage $b_1(t)$ when $|t|$ increases. This prediction is not supported from the present experiment since b_1 shows no t dependence (see Fig. 5 and Table VI).

In Tables III and IV and Fig. 3, we test two in-

TABLE VII. Energy dependence of the b, σ_{tot}, and ρ parameters. Parametrization in the form $P_i=A_i+B_i\ln(s_{p\mathrm{He}}/s_0)$, with $s_0=1$ GeV^2.

Parameter	A_i	B_i	$\chi^2/D.F.$
$b_{t=0}$ $[(\mathrm{GeV}/c)^{-2}]$	24.8 ± 1.3	1.13 ± 0.18	4/6
$b_{t=0}$ $[(\mathrm{GeV}/c)^{-2}]$, $c=-22$ $(\mathrm{GeV}/c)^{-4}$ fixed	24.9 ± 0.3	1.14 ± 0.04	10/6
$b_{t=0.035}$ $[(\mathrm{GeV}/c)^{-2}]$	26.2 ± 0.4	1.17 ± 0.05	15/6
$b_{t=0.065}$ $[(\mathrm{GeV}/c)^{-2}]$	26.6 ± 0.4	1.14 ± 0.06	7/6
$b_{t=0.095}$ $[(\mathrm{GeV}/c)^{-2}]$	28.6 ± 1.0	1.32 ± 0.10	23/6
$\sigma_{\mathrm{tot}}^{p\mathrm{He}}$ (mb)	108.7 ± 2.8	2.0 ± 2.8	14/6
$\rho_{t=0}$	-0.41 ± 0.1	0.059 ± 0.014	7/6

TABLE VIII. The parameters used in the calculation of $(d\sigma/dt)(p\,{}^4\mathrm{He})$. The corresponding curves are shown in Figs. 8, 9, and 11.

	One-particle density [Eq. (A5)]				Elementary amplitude [Eq. (A3)]							
Version	R_1^2 (GeV^{-2})	R_2^2 (GeV^{-2})	C	References	Energy (GeV)	σ_{tot} (mb)	ρ_0	ρ'	γ (GeV^{-2})	β	b_1 (GeV^{-2})	b_2 (GeV^{-2})
I	47.5		0		45	38.35	−0.150	0		0	10.72	
					301	39.56	−0.008	0		0	11.76	
					393	40.05	0.012	0		0	11.99	
II												
(i)	39.379	14.770	1	this work	45	38.35	−0.150	1	−0.44	0.42	12.21	7.64
(ii)	44.358	10.445	0.858	9	301	39.56	−0.008	1	−0.44	0.31	13.50	6.93
(iii)	42.946	6.136	1	21								

teresting predictions of geometric scaling. Geometric scaling, $\sigma_{tot}(E)$ proportional to $b(E)$, is satisfied (Fig. 3), but the other geometrical relation for the height of the second maximum, $(d\sigma/dt)(E, t_{\mathrm{sec\,max}})$ proportional to $\sigma_{tot}{}^2(E)$, is strongly violated since the function $(d\sigma/dt)(E)|_{\mathrm{sec\,max}}$ decreases and the function $\sigma_{tot}(E)$ rises with E.

VI. GLAUBER-MODEL ANALYSIS

Data from the whole t region, $0.003 \leq |t| \leq 0.52$ $(\mathrm{GeV}/c)^2$, were compared and fitted to the multiple-nucleon-scattering model, the Glauber model. In this model the full scattering amplitude is a coherent sum of single, double, triple, and quadruple scatterings from the four nucleons in ^{4}He.

In our analysis we have assumed that the nucleon-nucleon scattering amplitude is spin independent and the proton-proton and proton-neutron amplitudes are equivalent. Coulomb effects are neglected for $|t| > 0.05$ $(\mathrm{GeV}/c)^2$. We use a noncorrelated internal (or center-of-mass) wave function for the ^{4}He nucleus and identical one-particle density distributions for the protons and neutrons. No inelastic intermediate states are included in the parametrization.

Many of the details and parameter definitions are placed in the Appendix. The values of the parameters are listed in Table VIII. Two versions have been developed. For both of them comparison with the experimental data in the entire t range is done. In version I we calculated the nuclear amplitude in the simplest way identical with that described in Ref. 10. The phenomenological analysis of its parameters is performed in the small-t range. The more complex parametrization is done in version II.

Version I. In the small-t region the data may be successfully fitted with the following restrictive assumptions:

$$f_{\mathrm{nucleon}} = \frac{\sigma_{tot}}{4\pi}\, p(i+\rho)e^{-(b/2)q^2}, \tag{6}$$

$$\rho_i(\vec{r}_i) = \frac{\exp(-r_i{}^2/R_1{}^2)}{\pi^{3/2}R_1{}^3}, \tag{7}$$

where f_{nucleon} is the nucleon-nucleon amplitude, $\rho_i(\vec{r}_i)$ is the nucleon particle density, and $R_1 = 1.36$

TABLE IX. Parameters of the NN elastic-scattering amplitude as fitted by the Glauber model, version I, $|t| \leq 0.07$ $(\mathrm{GeV}/c)^2$. $\sigma_{\mathrm{tot}pp}$ is listed for comparison (from Ref. 14). Energy-dependent fits to the values of ρ and b are shown.

E_{lab} (GeV)	$\rho_{pp\,\mathrm{G1}}$	$b_{pp\,\mathrm{G1}}$ $[(\mathrm{GeV}/c)^{-2}]$	$\sigma_{\mathrm{tot\,G1}}$ (mb)	$\sigma_{\mathrm{tot}pp}$ (mb)	χ^2/DF
45	−0.087 ± 0.028	11.27 ± 0.14	35.22 ± 0.22	38.36	60/57
46	−0.062 ± 0.032	11.31 ± 0.16	35.08 ± 0.22	38.35	40/50
97	−0.090 ± 0.027	11.89 ± 0.14	34.78 ± 0.22	38.38	76/44
146	−0.049 ± 0.024	12.29 ± 0.12	35.31 ± 0.15	38.64	62/55
200	−0.022 ± 0.022	12.76 ± 0.12	35.45 ± 0.08	38.97	46/55
259	+0.024 ± 0.030	13.03 ± 0.13	35.88 ± 0.10	39.32	34/45
301	+0.031 ± 0.029	13.20 ± 0.12	35.58 ± 0.09	39.56	38/49
393	+0.067 ± 0.036	13.47 ± 0.16	36.38 ± 0.08	40.04	44/47

$\rho_{pp\,\mathrm{G1}} = -0.400 \pm 0.079 + (0.068 \pm 0.014)\ln(s_{pp}/s_0)$, $s_0 = 1\ \mathrm{GeV}^2$
$b_{pp\,\mathrm{G1}} = 6.63 \pm 0.38 + (1.03 \pm 0.07)\ln(s_{pp}/s_0)$

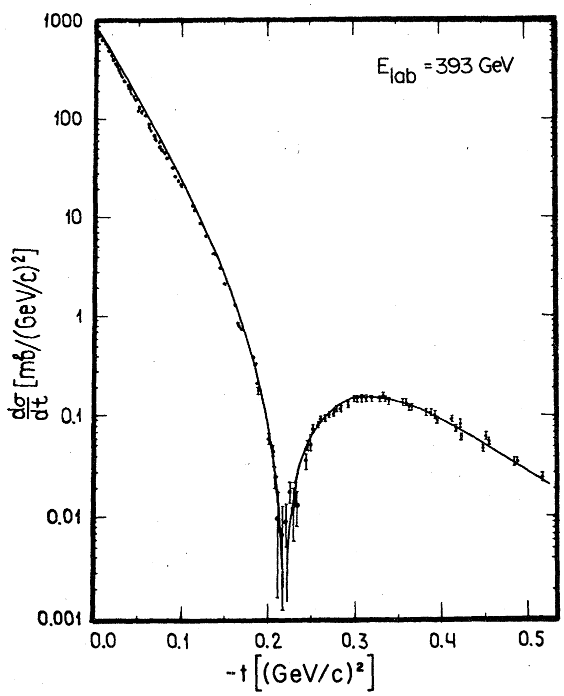

FIG. 8. The elastic differential $p\,^4$He cross section at 393 GeV. σ_{tot}, b, and ρ have been taken from pp experiments (Refs. 17 and 21) and listed in Table VIII. The solid line is the Glauber-model prediction with these parameters (version I). The Coulomb effect for $|t| < 0.03$ (GeV/c)^2 is extracted.

fm. The fitted parameters are b = slope parameter, ρ = ratio of the real to imaginary parts of the forward-scattering amplitude, and σ_{tot} = total nucleon-nucleon cross section; p is the proton laboratory momentum. We restrict the analysis range to $|t| < 0.07$ (GeV/c)^2. The results of these fits are given in Table IX. For comparison the values from the proton-proton experiment[17] are listed as well. In Fig. 7 the differential cross section at 393 GeV is shown. The fitted curve agrees well with the data, but at the expense of increasing b, and decreasing σ_{tot} from the known nucleon-nucleon values. The curve extrapolated into the wider t interval does not agree with the data in the region $|t| \gtrsim 0.22$ (GeV/c)^2. A similar discrepancy in the secondary maximum has been observed at lower energies,[1,2] and interpreted by some authors[9] as a consequence of a nonrealistic form of the wave function (Eq. 7).

Using the same formalism we calculate the differential cross section with fixed σ_{tot}, b, and ρ parameters taken from pp experiments. As an illustration Figs. 8, 9, and 11 show our 393, 45, and 301 GeV data compared with corresponding curves. The qualitative shape of the data is reproduced with a deep minimum and a secondary maximum, but the discrepancy between the data and theory is large at all energies, especially in the small-t region. A normalization change upwards would lessen this discrepancy.

Version II. For this more complex parametrization, many of the details are given in the Appendix. A double-Gaussian expression replaces the single-Gaussian expression in the nucleon-nucleon amplitude. In addition, ρ, the ratio of the real to the imaginary parts of the nucleon-scattering amplitude, is given a t (or q^2) dependence.

The choice of the wave-function parametrization is difficult. We have chosen a double-Gaussian expression taken from Refs. 9 and 21 [see Eq. (A5)

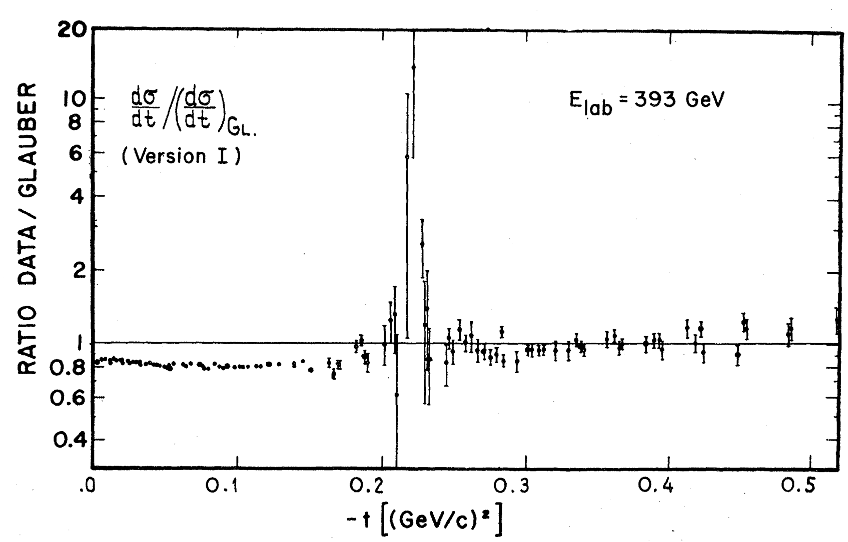

FIG. 9. The elastic differential cross section at 393 GeV shown as a ratio to the Glauber-model prediction (version I). σ_{tot}, b, and ρ values are those used with Fig. 8.

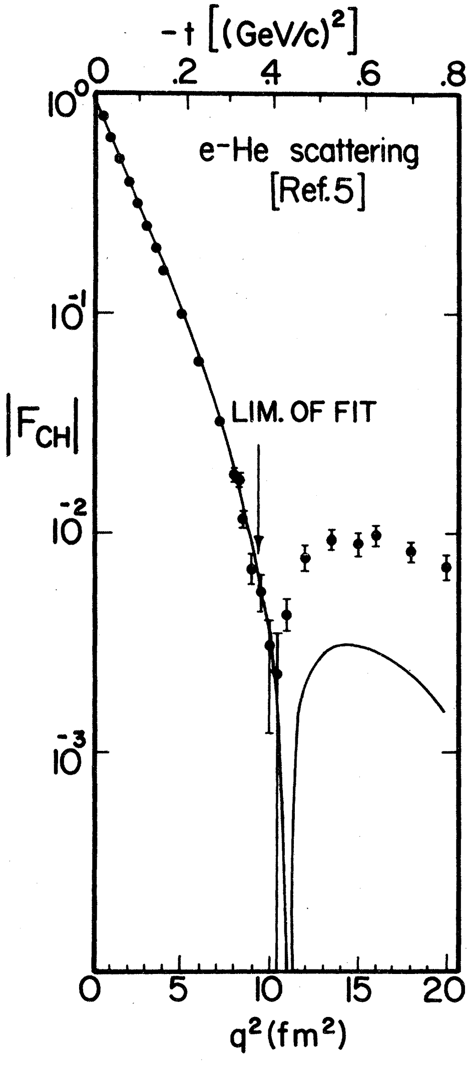

FIG. 10. The charge form factor of ^{4}He calculated from the single-particle wave function (A5). The parameters (see Table VIII) have been fitted to the data of Ref. 5 and 6 for $|t| \leq 0.35$ $(\mathrm{GeV}/c)^2$.

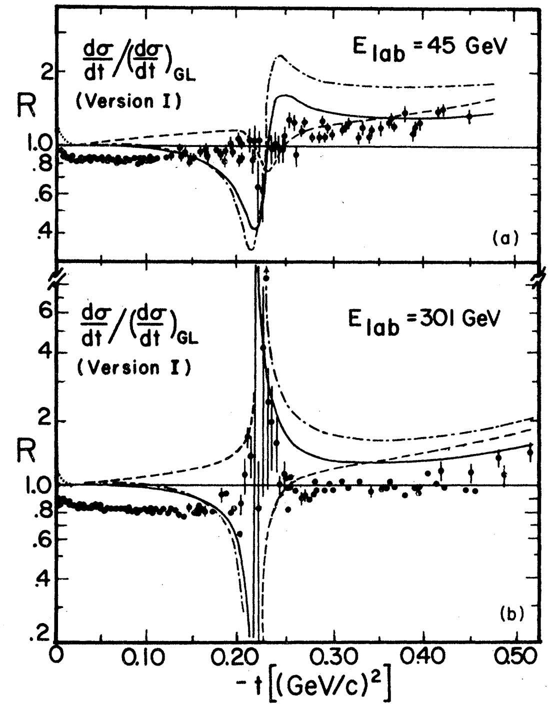

FIG. 11. The elastic p^4He differential cross section. All data points have been renormalized to the version I Glauber-model prediction. The curves show the results for various version II fitting procedures. Inelastic rescatterings are excluded in the analysis; the nucleon-nucleon amplitude is given by (A3). Three one-particle wave-function (A5) parametrizations are used: dot-dashed curve, our values for R_1, R_2, C [II(i)]: solid curve, Bassel-Wilkin [II(ii)], Ref. 9; dashed curve, Chou [II(iii)], Ref. 21. These three parametrizations are listed in Table VIII. The Coulomb effect in the small-t region is indicated by the dotted curve. (a) $E_{lab}=45$ GeV, (b) $E_{lab}=301$ GeV.

in the Appendix] containing three parameters R_1, R_2, and C. Different values of these parameters were used[9,22,23] to describe the same experimental electron-helium data.[5,6] Usually the efforts to fit better the position of the minimum and the magnitude of the second maximum of the ^{4}He form factor were made at the expense of a worse agreement with experimental data in the lower-t region. In order to calculate correctly the $p\,^4$He differential cross section in the relatively-small-t region, we obtained new values for the wave-function parameters from simultaneously fitting the two electron-^{4}He experiments of Ref. 5 and 6 for the limited region $q^2 \leq 9$ fm^{-2} [$|t| \leq 0.36$ $(\mathrm{GeV}/c)^2$]. Our fitted values are $R_1 = 39.4$ fm, $R_2 = 14.8$ fm; $C=1$ is found in the limit of the constraint $0 \leq C \leq 1$. The result of this $e\,^4$He fit is shown in Fig. 10.

In Figs. 11(a) and 11(b), we show the ratio of our version II curves to the curves of version I calculated at 45 and 301 GeV, respectively. Also shown are two additional curves where alternative parametrizations for the wave function are used; these are the Bassel-Wilkin[9] and the Chou[21] models. The agreement with the data is still not good. The three curves in Figs. 11(a) and 11(b) show the importance of the choice of the wave-function parametrization. The discrepancy between the data and theory in the very-small-t regions is 10–15%, as contrasted to the 4.8% total normalization error.

If we were to assume that the normalization error is higher than estimated (see Sec. III), one can try to reach a better agreement (between data

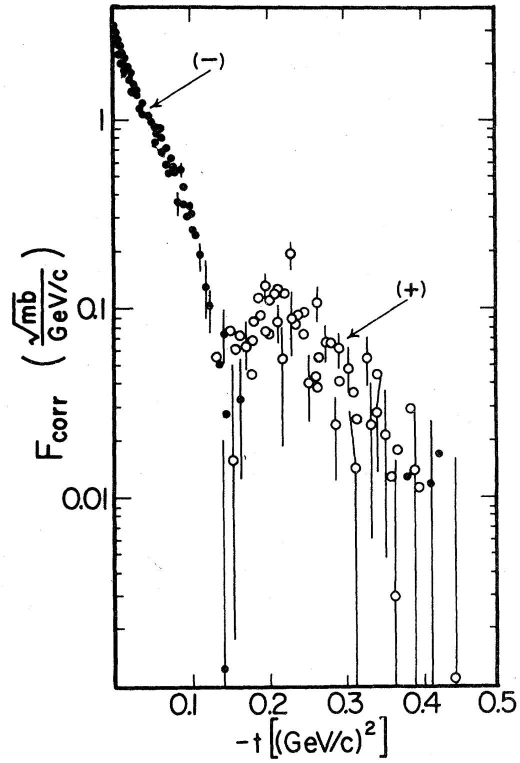

FIG. 12. The Glauber correction amplitude F_{corr} determined from the elastic differential cross section at 45 GeV. The Bassel-Wilkin parameters (Ref. 9) for the ^{4}He wave function have been used. The points ● have negative sign, the points ○ have positive sign.

and theory) by changing the normalization of the data. The change of the normalization causes a parallel shift of points in an up-down direction on the logarithmic scale of Figs. 11(a) and 11(b), but the differences in the shape of the curves and the data are still significant. It is very likely that the major cause of the failure of the version II parametrizations is the failure to include inelastic intermediate states in the double-, triple-, and quadruple-nucleon-rescattering terms. We have not pursued this matter further quantitatively because of the normalization difficulties mentioned previously but do suggest that the high energy and the accuracy of our data allow further analysis. Data on $A \neq 1$ targets are the only way to study the short-range interaction of N^* excited nucleon states.

Finally, we show the difference between the data and the Glauber-model calculation using amplitudes. Let us assume that the correction amplitude F_{corr}, satisfies the relation

$$\frac{d\sigma}{dt_{exp}} = |F_{Glauber} + F_{corr}|^2, \tag{8}$$

where $d\sigma/dt_{exp}$ is the experimental differential cross section. Assuming that

$$\mathrm{Re}(F_{corr}) = 0, \tag{9}$$

one can determine F_{corr} directly from experimental data as

$$F_{corr} = \pm\left(\frac{d\sigma}{dt_{exp}} - [\mathrm{Re}(F_{Glauber})]^2\right)^{1/2} - \mathrm{Im}(F_{Glauber}). \tag{10}$$

The result is shown in Fig. 12 [only one of two solutions of Eq. (10) is plotted]. In the calculation of $F_{Glauber}$ we use the Bassel-Wilkin wave-function parametrization [version II(ii)]. The analysis, similar to that made for pd and dd cases,[22] suggests that F_{corr} can be interpreted as an interference of rescatterings with intermediate inelastic states.

The inelastic screening correction at $t \simeq 0$ is estimated under the assumption that the discrepancy between the data and the Glauber-model prediction is mainly due to this effect. The contribution of the inelastic screening correction, $\Delta\sigma_{in}$, to the total cross section ($\sigma_{pHe} = 4\sigma_{pN} - \Delta\sigma_{el} - \Delta\sigma_{in}$) is ~9 mb which is ~15 times higher than in pd scattering and somewhat higher than the prediction given in Ref. 8.

VII. CONCLUSIONS

In this experiment, elastic $p\,^4$He scattering has been investigated in an energy range $45 \leq E_{lab} \leq 400$ GeV. The t interval $0.003 \leq |t| \leq 0.5$ (GeV/c)^2, where the differential cross section has been obtained, comprises the Coulomb-interference region, the forward diffraction peak, the Glauber minimum, and the second maximum. It contains about 80–120 data points at each primary proton energy and is measured with a typical relative statistical error of about 1.5–3%, except in the region of the minimum around $|t| \simeq 0.22$ (GeV/c)^2 where errors sometimes reach 50%.

The technique of the mixed hydrogen-helium jet target allows one to obtain absolute normalization of the differential cross section. The optical theorem is used to determine the total cross section for $p\,^4$He interactions. $\sigma_{tot}(E)$ rises for $E \geq 100$ GeV.

The parameters $\rho(s, t=0)$ and $b(s,t)$ of the $p\,^4$He scattering amplitude are obtained. The rate of shrinkage of the $p\,^4$He diffraction cone is more than twice as large as that for pp scattering. Geometrical scaling, $\sigma_{tot}(E)$ proportional to $b(E)$, is satisfied but the other geometrical relation for the height of the second maximum, $(d\sigma/dt)\,(E, t_{sec\,max})$ proportional to $\sigma_{tot}{}^2(E)$, is strongly violated.

The analysis of simple forms of the Glauber model show that substantial corrections to the elastic-scattering amplitude are needed. Inelastic screening seems to be important in the region of the diffractive cone as well as in the second maximum of the differential cross section. A more accurate estimation of the effect requires a better understanding of the ^{4}He wave function.

ACKNOWLEDGMENTS

We acknowledge the strong support of the Fermilab Internal Target Group led by Dr. Tom Nash, the Accelerator Division led by Dr. Russ Huson, and the Fermilab Computing Department led by Dr. Al Brenner. We are grateful to Professor Vladimir Kadeshevsky for his help. One of us (A.B.) thanks Dr. Z. Ajduk and Dr. L. Leśniak for helpful discussions. The Dubna members of the collaboration wish to acknowledge the support and hospitality of the Fermilab Directorate during their stay in the United States. Finally, the authors are grateful to their colleague, Dr. Andrzej Sandacz for his help. This work was supported in part by the U. S. Department of Energy, the U. S. National Science Foundation, and the U.S.S.R. State Committee for Atomic Energy.

APPENDIX

In this appendix we show the formalism of the multiple-scattering Glauber model and list some of the detailed parametrizations to which we have fitted our data; results are given in Sec. VI, Tables VIII and IX, and Figs. 7–12.

Defining the total density of the nucleus as a product of separate nucleon densities

$$\Psi^*\Psi = \prod_{i=1}^{4} \rho_i(\vec{r}_i) \quad \text{with} \int \rho_i(\vec{r}_i)\, d^3r_i \equiv 1\,, \tag{A1}$$

we derive the nuclear amplitude from the Glauber model:

$$\begin{aligned} F(\vec{\Delta}) = {} & 4f(\vec{\Delta})\,G(\tfrac{3}{4}\vec{\Delta})\,G(-\tfrac{1}{4}\vec{\Delta}) - 6\frac{G^2(-\vec{\Delta}/4)}{2\pi i p}\int d^2q\, f(\tfrac{3}{4}\vec{\Delta}-\vec{q})\, f\!\left(\frac{\vec{\Delta}}{4}+\vec{q}\right) G\!\left(\frac{\vec{\Delta}}{2}-\vec{q}\right) G(\vec{q}) \\ & + 4\frac{G(-\vec{\Delta}/4)}{(2\pi i p)^2}\int d^2q_1 d^2q_2\, f\!\left(\frac{\vec{\Delta}}{4}+\vec{q}_1\right) f\!\left(\frac{\vec{\Delta}}{4}+\vec{q}_2\right) f\!\left(\frac{\vec{\Delta}}{2}-\vec{q}_1-\vec{q}_2\right) G(\vec{q}_1)\,G(\vec{q}_2)\,G\!\left(\frac{\vec{\Delta}}{4}-\vec{q}_1-\vec{q}_2\right) \\ & - \frac{1}{(2\pi i p)^3}\int d^2q_1 d^2q_2 d^2q_3\, f\!\left(\frac{\vec{\Delta}}{4}+\vec{q}_1\right) f\!\left(\frac{\vec{\Delta}}{4}+\vec{q}_2\right) f\!\left(\frac{\vec{\Delta}}{4}+\vec{q}_3\right) f\!\left(\frac{\vec{\Delta}}{4}-\vec{q}_1-\vec{q}_2-\vec{q}_3\right) \\ & \times G(\vec{q}_1)\,G(\vec{q}_2)\,G(\vec{q}_3)\,G(-\vec{q}_1-\vec{q}_2-\vec{q}_3)\,. \end{aligned} \tag{A2}$$

The Fourier transform of the one-particle density is

$$G(\vec{q}) = \int e^{i\vec{q}\cdot\vec{r}} \rho_i(\vec{r})\, d^3r\,.$$

$\vec{\Delta}$ and $\vec{q}$ are the vectors of the transverse momentum transfers to the nucleus and to the nucleon, respectively, p is the laboratory momentum of the projectile, and $\vec{r}_i$ is the position of the ith nucleon in the c.m. system of the nucleus. Formula (A2) contains the constraint associated with the uniform motion of the nuclear center of mass. The amplitude F is normalized as

$$\frac{d\sigma}{dt} = \left|\frac{\sqrt{\pi}}{p}F\right|^2,$$

where $-t = q^2$. The nucleon-nucleon amplitude is parametrized in the form

$$f(q) = \frac{\sigma_{\text{tot}}}{4\pi}\, p[i+\rho(q)]\,\frac{e^{-(b_1/2)q^2} + \beta\, e^{-(b_2/2)q^2}}{1+\beta}\,, \tag{A3}$$

where σ_{tot} is the nucleon-nucleon total cross section and $\rho(q)$, the ratio of the real to imaginary parts of the amplitude, is

$$\rho(q) = \frac{\operatorname{Re} f(q)}{\operatorname{Im} f(q)} = \rho(0) + \rho'(e^{\gamma q^2} - 1) \tag{A4}$$

and b_1, b_2, β, ρ, and γ are all arbitrary parameters.

For the one-particle density we take the form of a double Gaussian proposed by Bassel and Wilkin,[9] and Chou[21]:

$$\rho_i(\vec{r}_i) = K\left[\exp\left(-\frac{\vec{r}_i^{\,2}}{R_1^2}\right) - C\exp\left(-\frac{\vec{r}_i^{\,2}}{R_2^2}\right)\right] \tag{A5}$$

with

$$K = \pi^{-3/2}(|R_1|^3 - C|R_2|^3)^{-1}\,,$$

where K is the normalization factor. R_1, R_2, and C are free parameters, which can be deduced from the charge form factor of the ^{4}He nucleus. The Gaussian form of Eqs. (A3), (A4), and (A5) has been chosen partially in order to simplify the necessary integrations. The Fourier transform of Eq. (A5) is

$$G(\vec{q}) = \frac{1}{1-D}\left[\exp\left(-\frac{R_1^2 q^2}{4}\right) - D\exp\left(-\frac{R_2^2 q^2}{4}\right)\right] \quad \text{(A6)}$$

with

$$D = C(R_2/R_1)^3 .$$

Inserting Eqs. (A3) and (A6) into Eq. (A2), we may calculate the differential cross section in two ways.

Version I.

$$\beta, D, \rho' = 0 .$$

In this case the amplitude F [Eq. (A2)] takes a well-known form.[10] The parameters $b = b_{pp}$, $\rho = \rho_{pp}(t=0)$, and $\sigma_{\text{tot}} = \sigma_{\text{tot}}^{pp}$ are fixed by pp experiments[14,19] or treated as variable parameters. The parameter $R_1 = 1.36$ fm.[23]

Version II. A more realistic version for calculation is to take into account more complex expressions for the nucleon-nucleon amplitude and a more realistic expression for the charge form factor of ^{4}He nucleus.

The parameters β, b_1, b_2 of the elementary amplitude have been determined as follows.

(i) The experimental pp data have been interpolated to our energies using the known[19,24] energy dependence of the parameters.

(ii) The reconstructed differential cross sections have been fitted using our parametrization (A4) with fixed values of $\rho' = 1$, and $\gamma = -0.44$ (GeV/c)^2. We have assumed here that the amplitude ratio (A4) is approximated as

$$\rho(t) = \frac{\operatorname{Re} f(t)}{\operatorname{Im} f(t)} = \rho_0^{pp}(s, t=0) + \tfrac{1}{2}\pi[\alpha_{\text{Pomeron}}(t) - 1]$$

$$\simeq \rho_0^{pp} + 0.44\,t \simeq \rho_0^{pp} + (e^{0.44t} - 1) , \quad \text{(A7)}$$

where $\alpha_{\text{Pomeron}} = 1 + 0.278\,t$.

---

*Some portions of this paper were prepared by A. Bujak for submission in partial fulfillment of the requirements for a Ph.D. degree.

†Present address: Purdue University, Lafayette, Indiana 47907.

‡Permanent address: Institute of Technology and Chemistry, Sofia, Bulgaria.

§Permanent address: KEK, Ibaraki-ken, Japan.

[1] See, e.g., the review by G. Igo, in *High Energy Physics and Nuclear Structure—1975*, proceedings of the Sixth International Conference, Santa Fe and Los Alamos, edited by D. E. Nagle and A. S. Goldhaber (AIP, New York, 1975), p. 63.

[2] J. Berthot *et al.*, Clermont-Ferrand–Lyon–Strasbourg Collaboration, preliminary results as reported at various conferences, e.g., *High Energy Physics and Nuclear Structure*, proceedings of the Fifth International Conference, Uppsala, Sweden, 1973, edited by G. Tibell (North-Holland, Amsterdam, 1974).

[3] Dubna- Warsaw-Leningrad Collaboration, Yad. Fiz. 27, 710 (1978) [Sov. J. Nucl. Phys. 27, 380 (1978)].

[4] V. G. Ableev *et al.*, Yad. Fiz. 28, 1529 (1978) [Sov. J. Nucl. Phys. 28, 786 (1978)].

[5] R. F. Frosch *et al.*, Phys. Rev. 160, 874 (1967).

[6] F. C. McCarthy *et al.*, Phys. Rev. 15C, 1396 (1977).

[7] T. Ekelöf *et al.*, Nucl. Phys. B35, 495 (1971).

[8] E. M. Levin and M. I. Strikman, Leningrad Nuclear Physics Institute Report No. 203, 1975 (unpublished).

[9] R. Bassel and W. Wilkin, Phys. Rev. 174, 1179 (1968).

[10] W. Czyż and L. Leśniak, Phys. Lett. 24B, 227 (1967).

[11] W. Czyż and L. C. Maximon, Phys. Lett. 27B, 354 (1968).

[12] J. Auger *et al.*, Nucl. Phys. A262, 372 (1976).

[13] A. Bujak *et al.*, following paper, Phys. Rev. D 23, 1911 (1981).

[14] A. S. Carrol *et al.*, Phys. Rev. Lett. 33, 928 (1974).

[15] A. Schiz *et al.* (unpublished).

[16] J. P. Burq *et al.*, preliminary results presented at the XXth International Conference on High Energy Physics, Madison, Wisconsin, 1980 (unpublished).

[17] E. Jenkins *et al.*, preliminary results from this experiment presented at the 19th International Conference on High Energy Physics, Tokyo, 1978 (unpublished); also quoted in rapporteur talk by V. A. Nikitin, in *Proceedings of the European Physical Society International Conference on High Energy Physics, Geneva, Switzerland, 1979,* edited by A. Zichichi (CERN, Geneva, 1980), pp. 547–567.

[18] H. Bethe, Ann. Phys. (N. Y.) 3, 190 (1958).

[19] D. Gross *et al.*, Phys. Rev. Lett. 41, 217 (1978).

[20] Yu. Y. Azimov *et al.*, Pis'ma Zh. Eksp. Teor. Fiz. 23, 131 (1975) [JETP Lett. 23, 114 (1976)].

[21] T. T. Chou, Phys. Rev. 168, 1594 (1968).

[22] G. Goggi *et al.*, Nucl. Phys. B149, 381 (1979).

[23] E. Lambert and H. Feshbach, Ann. Phys. (N. Y.) 76, 80 (1973), p. 102.

[24] D. S. Ayres *et al.*, Phys. Rev. D 15, 3105 (1977).